24th COBEM - 2017

24th ABCM International Congress of Mechanical Engineering
December 3-8, 2017, Curitiba, PR, Brazil

COBEM-2017-1038
VALIDATION OF A LIMITING METHODOLOGY FOR HIGH-ORDER METHODS

Marco Aurélio Leonel Matunaga
Fábio Mallaco Moreira
Instituto Tecnológico de Aeronáutica, DCTA/ITA, São José dos Campos, SP, Brazil
marco.matunaga@gmail.com, fabiom91@gmail.com

João Luiz F. Azevedo
Instituto de Aeronáutica e Espaço , DCTA/IAE/ALA, São José dos Campos, SP, Brazil
joaoluiz.azevedo@gmail.com

Abstract. *High-order methods are interesting to the CFD community due to their increased solution accuracy at comparable costs. One of the major concerns in the application of these numerical schemes is the degradation of the numerical solution by flow discontinuities, such as shock waves. Thus, for simulating high speed compressible flows, it is necessary to introduce a mechanism to handle these numerical instabilities. In the present paper, the authors evaluate a new limiting technique, recently proposed for the CPR method, adapting it to the Spectral Difference method. The proposed limiter is studied through its applications to both standard high-order CFD validation test cases and traditional aeronautical flows. It is expected that new limiter can provide improved convergence properties while preserving the smoothness of the solution.*

Keywords: *CFD, High-order methods, Limiters, Transonic Flow, Aerodynamics*

1. INTRODUCTION

High-order methods, defined as at least third-order accurate methods, could provide more accurate results with lower cost than low order methods (Wang *et al.*, 2013). For this reason high-order CFD methods are attracting the attention of many CFD laboratories. The main goal of the present study is develop and test a limiter for a higher-order scheme. A problem concerned to these methods are the discontinuities, such as the shock waves typically present in aerospace-type flows. There are two approaches typically used in order the handle the numerical difficulties created by such discontinuities, namely, the use of artificial viscosity or the implementation of a limiter function. The artificial viscosity approach introduces additional dissipation term in the governing equations near the discontinuities to smooth out the oscillations caused by these discontinuities. The perceived problem with this approach is that, usually, it needs parameters which could not be used by all problems and the stability for explicit time stepping methods is not good.

The limiter approach, in the present case, is an extension to high-order methods of the ideas developed by van Leer (1979) for the MUSCL scheme. As in the original concept, the main idea is the use of the limiter in regions near the discontinuities, avoiding the degradation of the smooth solution. Clearly, however, the limiter must be formulated such that it does not immediately reverts to 1st-order accuracy every time an extremum is found, as this behavior would lead to too much limiting (Breviglieri *et al.*, 2010). Another concern with limiters is the convergence to steady state problems, as the highly nonlinear scheme, with the presence of the limiter, tends to suffer from convergence stall. The limiter used in the present study is an adaptation of the approach recently proposed by Li and Wang (2017) for the Correction Procedure via Reconstruction (CPR) method. In the present work, such approach is reinterpreted in the spectral difference method context. Moreover, Li and Wang's limiter, on the other hand, was developed based on the work of Michalak and Ollivier-Gooch (2009), who developed a limiter for high-order finite volume schemes.

2. SPECTRAL DIFFERENCE METHOD

The flows of interest in the present work are assumed to be adequately modeled by the 2-D Euler equations. The Euler equations describe the most general flow configuration for a non-viscous, non-heat conducting fluid. They are formed by the combination of three conservation laws, namely the conservation of mass, the momentum equations and conservation of energy, that are combined with the equation of state for perfect gases to form a closed system. These equations can be

written in differential form as

$$\frac{\partial Q}{\partial t} + \frac{\partial E_e}{\partial x} + \frac{\partial F_e}{\partial y} = 0 \,. \tag{1}$$

The vector of conserved variables, Q, and the convective flux vectors, E_e and F_e, are given by

$$Q = \left\{ \begin{array}{c} \rho \\ \rho u \\ \rho v \\ \varepsilon \end{array} \right\} , \qquad E_e = \left\{ \begin{array}{c} \rho u \\ \rho u^2 + p \\ \rho uv \\ (\varepsilon + p)u \end{array} \right\} , \qquad F_e = \left\{ \begin{array}{c} \rho v \\ \rho uv \\ \rho v^2 + p \\ (\varepsilon + p)v \end{array} \right\} . \tag{2}$$

The aforementioned equation of state for perfect gases can be written as

$$p = (\gamma - 1) \left[\varepsilon - \frac{1}{2} \rho (u^2 + v^2) \right] , \tag{3}$$

where ε is the total energy per unit volume and the ratio of specific heats, γ, is set as 1.4 for all computations in this work.

The spectral difference (SD) method employs a finite difference-like scheme. In order to achieve an efficient implementation, all cells in the physical domain, (x, y), are transformed into a unit square element in the computational domain. Such transformation can be written as

$$\left(\begin{array}{c} x \\ y \end{array} \right) = \sum_{s=1}^{K} M_s(\xi, \eta) \left(\begin{array}{c} x_s \\ y_s \end{array} \right) , \tag{4}$$

where K is the number of points used to define the physical element, (x_s, y_s) are the Cartesian coordinates of such points, and $M_s(\xi, \eta)$ are the shape functions of the geometric transformation. In the case of a 1st-order linear boundary mesh, the transformation is bilinear and the analytic expression can be easily found. However, in the case of higher order meshes, required to accurately represent curved geometries, the number of points used to define a single cell increases. Considering a bi-polynomial representation, the transformation parameters can be calculated by numerically solving a linear system of size K.

The metric terms and the Jacobian matrix of the transformation can be computed in a pre-processing step and kept in memory given the stationary aspect of the mesh for the problems here considered. The implementation follows the formulation presented in Refs. Wang *et al.* (2007) and May and Jameson (2006). The governing equations in the physical domain are transformed into the computation domain and are rewritten as

$$\frac{\partial \widetilde{Q}}{\partial t} + \frac{\partial \widetilde{E_e}}{\partial \xi} + \frac{\partial \widetilde{F_e}}{\partial \eta} = 0 \,, \tag{5}$$

where $\widetilde{Q} = |J| \, Q$ and J is the Jacobian matrix of the coordinate transformation, given by

$$J = \left(\begin{array}{cc} x_\xi & x_\eta \\ y_\xi & y_\eta \end{array} \right) . \tag{6}$$

For the current implementation, the flux vectors in the computational domain can be simplified from the general form as

$$\begin{aligned} \left(\begin{array}{c} \widetilde{E_e} \\ \widetilde{F_e} \end{array} \right) &= \left(\begin{array}{cc} x_\xi & x_\eta \\ y_\xi & y_\eta \end{array} \right)^{-1} \left(\begin{array}{c} E_e(Q) \\ F_e(Q) \end{array} \right) \\ &= |J| \cdot \left(\begin{array}{cc} \xi_x & \xi_y \\ \eta_x & \eta_y \end{array} \right) \left(\begin{array}{c} E_e \\ F_e \end{array} \right) \\ &= \left(\begin{array}{cc} y_\eta & -x_\eta \\ -y_\xi & x_\xi \end{array} \right) \left(\begin{array}{c} E_e \\ F_e \end{array} \right) . \end{aligned} \tag{7}$$

In the standard element, two sets of points are defined, namely the solution points (SP) and the flux points (FP). As shown in Ref. Van den Abeele *et al.* (2008), the stability of the method in a large array of problems is independent from the distribution of the SPs, meaning another criteria may be used in order to determine the location of these points. If, for instance, memory usage is a concern, SPs could be made to coincide with FPs, hence minimizing memory allocation. In the present implementation, the favored aspects are simplicity of implementation for computational efficiency. Therefore, an internal cell discretization that only requires dealing with one-dimensional problems is selected. The use of tensor products and the enforcement that the directions of the interpolations and derivatives should coincide greatly simplify the formulation of the method. An example of such distribution, for a 3rd-order SD scheme, is illustrated in Fig. 1.

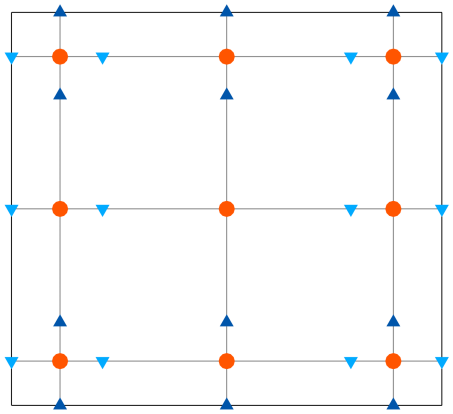

Figure 1. Possible solution point (orange circles) and flux points (blue triangles) distribution for the 3rd-order SD method.

The number of points in a cell is determined by the order of the interpolating polynomial required to achieve the desired accuracy. For an n-th order method, n^2 SPs are required, such that, in each direction, there are n points and an $n-1$ degree polynomial can be reconstructed. In order to avoid the weak instability caused by using a Chebyshev-Gauss linear distribution (Van den Abeele *et al.*, 2008), the SPs are chosen to be the Gauss-Legendre points, which are defined as the roots of the Legendre polynomial of order n,

$$P_n(\xi) = \frac{1}{2^n}\sum_{s=0}^{n}\left[\binom{n}{s}(\xi-1)^{n-s}(\xi+1)^s\right] \tag{8}$$

shifted from the interval $[-1,1]$ to $[0,1]$. In order to preserve the solution accuracy, n-degree polynomials are used to interpolate the fluxes and, hence, the $n+1$ flux points are selected to be the Legendre-Gauss-Lobatto points, defined by the roots of the Legendre polynomial of order $n-1$ plus the end points of the interval, similarly shifted to suit the $[0,1]$ interval.

Using the solution at n solution points, an $(n-1)$ degree polynomial can be built using the following Lagrange basis, defined as

$$g_i(\xi) = \prod_{s=1,\, s\neq i}^{n}\left(\frac{\xi-\xi_s}{\xi_i-\xi_s}\right). \tag{9}$$

Similarly, using the flux values at $(n+1)$ flux points, an n degree polynomial can be built for the flux using a similar Lagrange basis, defined as

$$l_{i+\frac{1}{2}}(\xi) = \prod_{s=0,\, s\neq i}^{n}\left(\frac{\xi-\xi_{s+\frac{1}{2}}}{\xi_{i+\frac{1}{2}}-\xi_{s+\frac{1}{2}}}\right). \tag{10}$$

The reconstructed solution for the conserved variables in the standard cell is given by the tensor product of the two 1-D polynomials,

$$Q(\xi,\eta) = \sum_{i=1}^{n}\sum_{j=1}^{n}\frac{\widetilde{Q}_{i,j}}{|J_{i,j}|}\, g_i(\xi)\cdot g_j(\eta)\,, \tag{11}$$

where $\widetilde{Q}_{i,j}$ represents the values of the conserved properties at the SPs. Similarly, the reconstructed flux polynomials take the following form

$$\widetilde{E}(\xi,\eta) = \sum_{i=0}^{n}\sum_{j=1}^{n}\widetilde{E}_{i+\frac{1}{2},j}\cdot l_{i+\frac{1}{2}}(\xi)\cdot g_j(\eta)\,, \tag{12}$$

$$\widetilde{F}(\xi,\eta) = \sum_{i=1}^{n}\sum_{j=0}^{n}\widetilde{F}_{i,j+\frac{1}{2}}\cdot g_i(\xi)\cdot l_{j+\frac{1}{2}}(\eta)\,, \tag{13}$$

where $\widetilde{E}_{i+\frac{1}{2},j}$ and $\widetilde{F}_{i,j+\frac{1}{2}}$ are the values of the flux vectors at the corresponding FPs.

The reconstructed variables are element-wise continuous, but discontinuous across cell interfaces. On the internal FPs, the flux can be directly calculated from the conserved variables interpolated from the SPs. However, in order to ensure stability and conservation, a common numerical flux must be determined for both neighboring cells at their interface, and this can be done by using a Riemann solver. In this work, the Roe approximate Riemann solver is used as numerical flux function for the inviscid fluxes.

Once the polynomial interpolation for the fluxes has been constructed, the derivatives of the fluxes are computed at the solution points using the derivatives of the Lagrange operators, l, as

$$\frac{\partial \widetilde{E}}{\partial \xi} = \sum_{i=0}^{n} \sum_{j=1}^{n} \widetilde{E}_{i+\frac{1}{2},j} \cdot l'_{i+\frac{1}{2}}(\xi) \cdot g_j(\eta) \,, \tag{14}$$

$$\frac{\partial \widetilde{F}}{\partial \eta} = \sum_{i=1}^{n} \sum_{j=0}^{n} \widetilde{F}_{i,j+\frac{1}{2}} \cdot g_i(\xi) \cdot l'_{j+\frac{1}{2}}(\eta) \,. \tag{15}$$

With the gradients of the fluxes calculated on the SPs, an explicit or an implicit time-stepping method can be invoked. The explicit scheme implemented here is the explicit 2nd-order, 3-stage optimal strong stability preserving Runge-Kutta scheme described in Ref. Spitieri and Ruuth (2003). The implicit time-marching methods, which are the main interest in the present paper, are discussed in the next section. Local time stepping is used for all cases, and the characteristic length used in the CFL number calculation of each cell is the average of all four sides of the cell faces.

3. LIMITER

The limiter addressed in the present paper is an extension of the formulation originally proposed by Li and Wang (2017) for the Correction Procedure via Reconstruction (CPR) method, also called Flux Reconstruction (FR) method. A description of the adaptation of this limiter to the present implementation of the SD method is presented in this section.

3.1 Limiter Function

In the SD method the solution in each cell is represented by a polynomial of the form

$$Q(\xi,\eta) = \sum_{i=1}^{n} \sum_{j=1}^{n} \frac{\widetilde{Q}_{i,j}}{|J_{i,j}|} \, g_i(\xi) \cdot g_j(\eta), \tag{16}$$

as shown in the previous section. When approximating discontinuous solutions this polynomial interpolation can become unstable and oscillatory. The limiter is introduced in the spatial discretization in order to stabilize the numerical method in these critical points.

To guarantee that the local solution reconstruction is not oscillatory we limit its maximum and minimum values in the current cell to the interval $[\min(\overline{Q}_k^{\,neighbor}), \max(\overline{Q}_k^{\,neighbor})]$, where $\overline{Q}_k^{\,neighbor}$ denotes the average of the solution reconstruction in the face neighboring cells of k, including cell k itself. If the solution reconstruction in cell k is not contained in this interval then it needs to be limited.

Limiting is performed by compressing the reconstructed solution around the cell average following the equation

$$Q_k = \overline{Q}_k + \Phi_k\,(1,y)\,\left(Q_k - \overline{Q}_k\right) \tag{17}$$

where Φ is a compression coefficient based on the maximum deviation of the local reconstruction from the cell average solution which is named y and defined by

$$y = \max\left(\frac{\max(\overline{Q}_k^{\,neighbor}) - \overline{Q}_k}{\max(Q_k) - \overline{Q}_k}, \frac{\min(\overline{Q}_k^{\,neighbor}) - \overline{Q}_k}{\min(Q_k) - \overline{Q}_k}\right). \tag{18}$$

As presented by Michalak and Ollivier-Gooch (2009) it is beneficial to use a smooth and differentiable limiting function Φ to prevent the limiter from switching on and off in critical regions which usually causes a stall in convergence. This function can be determined by solving an ODE with the appropriate boundary conditions as to enforce that the function is contained in the TDV region $P(y) \leqslant min(1,y)$. This function can be defined as

$$\Phi_k\,(1,y) = \begin{cases} P(y), & y < y_t \\ 1, & y \geqslant y_t \end{cases} \tag{19}$$

where $P(y)$ is a polynomial satisfying the conditions

$$P|_{y_0} = y_0, \quad \frac{dP}{dy}|_{y_0} = 1, \quad P|_{y_t} = 1, \quad \frac{dP}{dy}|_{y_t} = 1, \quad \forall y \in [y_0, y_t]. \tag{20}$$

The resulting polynomial for $y_0 = 0$, $y_t = 1.5$ is

$$P(y) = -\frac{4}{27}y^3 + y \tag{21}$$

3.2 Smooth Region Correction

While the limiting function assures the numerical stability of the method it can be adversely affect the accuracy of the solution near smooth extrema. Therefore it is necessary to turn off the limiter in smooth regions to obtain high-order accuracy and good numerical convergence.

Using the smoothness indicator proposed by Persson and Peraire (2006) the smoothness of the local reconstruction can be assessed and limiter properly applied. The smoothness indicator S_k is defined as

$$S_k = log_{10}\left(\frac{|Q_k - \widehat{Q}_k|_2}{|Q_k|_2}\right) , \tag{22}$$

where the norm is defined by the standard inner product for functions and $\widehat{Q}_k$ is the L_2 projection of the solution reconstruction in a one degree lower polynomial space, i.e.

$$\widehat{Q}_k = \sum_{i=1}^{n-1}\sum_{j=1}^{n-1} Q_{i,j} \cdot \ g_i(\xi) \cdot g_j(\eta). \tag{23}$$

To make a smooth transition between the fully limited and not limited solution regions, σ_k is introduced, being defined as

$$\sigma_k = \begin{cases} 1, & S_k \leqslant S_0 - \kappa \\ \frac{1}{2}\left(1 - sin\left(\frac{\pi}{2}\frac{S_k - S_0}{\kappa}\right)\right), & S_0 - \kappa < S_k < S_0 + \kappa \\ 0, & S_k \geqslant S_0 + \kappa \end{cases} . \tag{24}$$

The final limiting parameter is, therefore, of the following form

$$\widetilde{\Phi}_k = \sigma_k + (1 - \sigma_k)\Phi_k , \tag{25}$$

and the limited reconstruction becomes

$$Q_k = \overline{Q}_k + \widetilde{\Phi}_k\,(1, y)\left(Q_k - \overline{Q}_k\right). \tag{26}$$

4. RESULTS

The new limiting procedure is compared with results obtained with other limiter previously studied by the authors. The following cases are analyzed: supersonic flow in a duct and transonic flow simulation around a NACA 0012 airfoil. Further details of the definition of the test cases that are considered here can be seen in Ref. Moreira *et al.* (2015). Moreover, special attention is given to comparisons with the hierarchical limiter, previously used with the SD method by the authors, which was developed by Yang and Wang (2009). A detailed description of this limiter and its application to the SD method is shown in Ref. Moreira *et al.* (2016). In the next sections, a description of the test cases for the present work is given.

4.1 NACA 0012 Airfoil

The flow over a NACA 0012 airfoil is simulated. Freestream conditions are defined as $M_\infty = 0.8$ and $\alpha = 0$ deg. A C-type mesh is used, which contains 4619 quadrilaterals and 108 edges over the airfoil surface. The distance to the farfield is 10 chord-lengths. A view of the computational mesh near the airfoil is shown in Fig. 2.

Results for transonic flow around the NACA 0012 airfoil are shown in Fig. 3. The calculations are performed with a 3rd-order SD method, using the hierarchical limiter proposed in Ref. Yang and Wang (2009). In the figure, one can see density contours as well as a visualization of the limited cells at the last iteration of the convergence process. It is clear from the left-hand side plot in Fig. 3 that some cells are being limited in the smooth regions of the flow. The solution is still good, as one can see in the right-hand side plot, but the fact that the limiter is marking cells in the smooth regions of the flow is an indication that there is a need for improvement in the limiter formulation, which is precisely the motivation for the present effort. Furthermore, previous work, reported in Ref. Moreira *et al.* (2015), has identified that there are problems with the convergence rate for this test case with the hierarchical limiter. This observation, together with the sensitivity of limiter in smooth regions of the flow, is another indication of the need for future work.

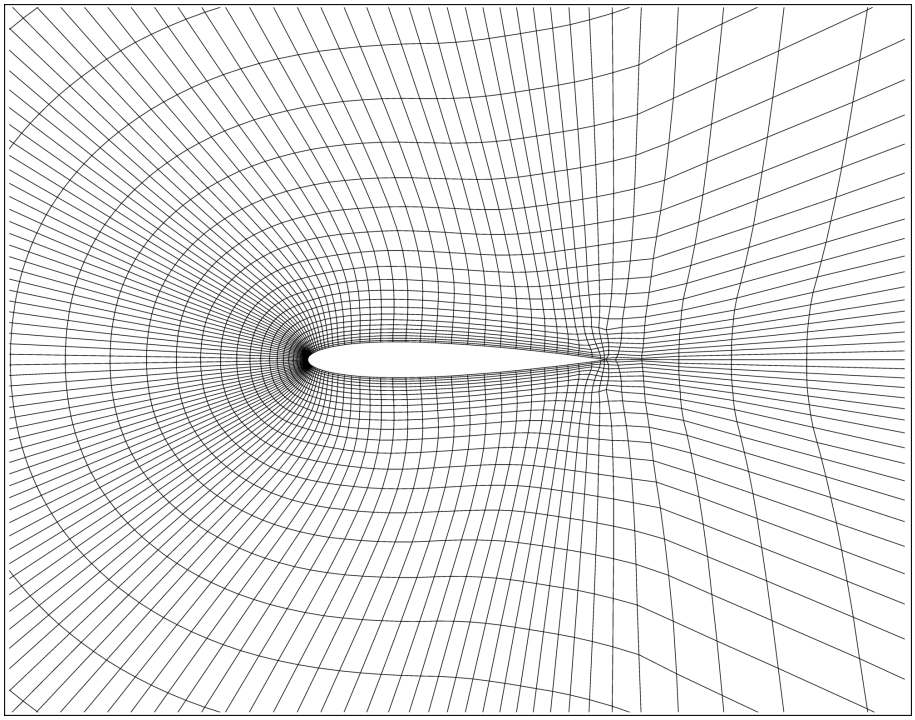

Figure 2. Mesh used for the SD method NACA 0012 airfoil simulations.

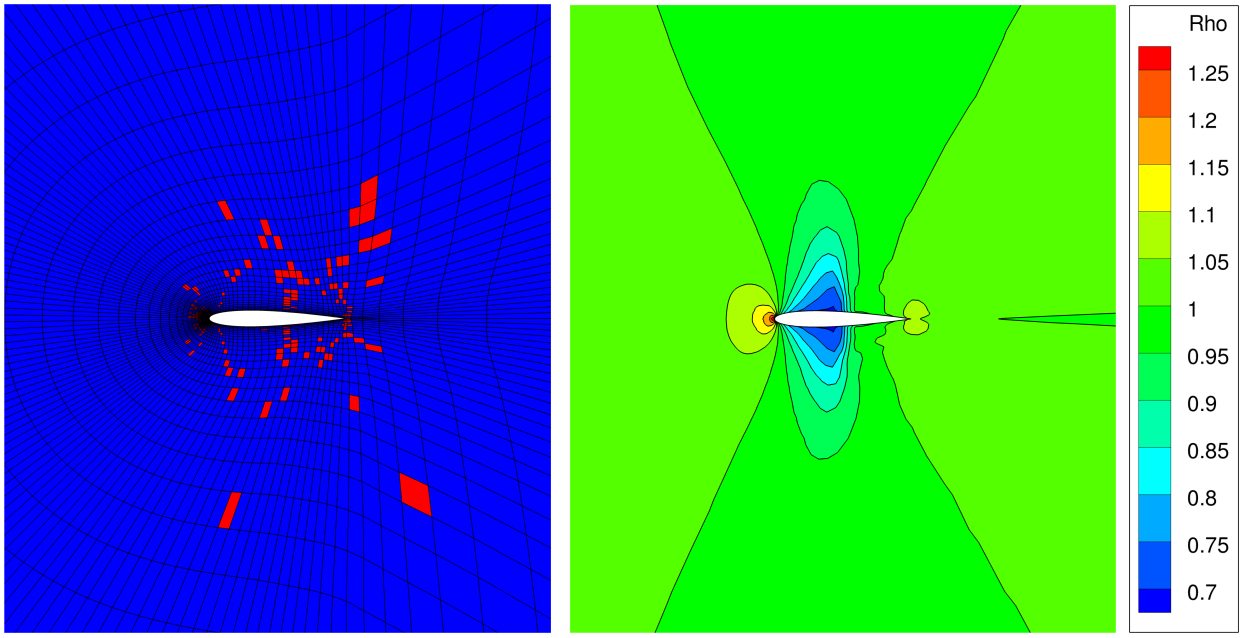

(a) Limited cells for density reconstruction (red). (b) Density contours.

Figure 3. Results for the SD method NACA 0012 airfoil simulations at $M_\infty = 0.8$ and $\alpha = 0$ deg.

The results obtained with spectral difference with the limiter described in the present article are shown in the Fig. 4. In the leftmost figure it shown the limited cells for the density values. As described earlier in the Eq. 25, the limiting parameter varies from 0 to 1. This scale means that the cell will be fully limited when the value reaches zero and will not limited when this parameter is one. For the present simulation, the minimum value of the final limiting parameter is about 0.9, which means a minor compression of the cell values.

In the far left figure, the values of the cells near the wall are also limited. This fact suggests that the wall influences in the limiting function, which is a minor drawback for this procedure. A positive aspect of this limiting technique is that the cells in the smooth solution was practically not limited. So, the limiter function not degrades the smooth solution,

differently of the previous methodology, as the results presented in Fig. 3, which is an improvement in the numerical scheme from other simulations in Moreira *et al.* (2015) and Moreira *et al.* (2016) whose limiter was the hierarchical developed by Yang and Wang (2009).

The figure of density contours shows a well-defined shock. This result represents another improvement considering the results obtained earlier with the hierarchical limiter. As seen in Fig. 3 the shock in the NACA0012 airfoil was not well represented as in Fig. 4.

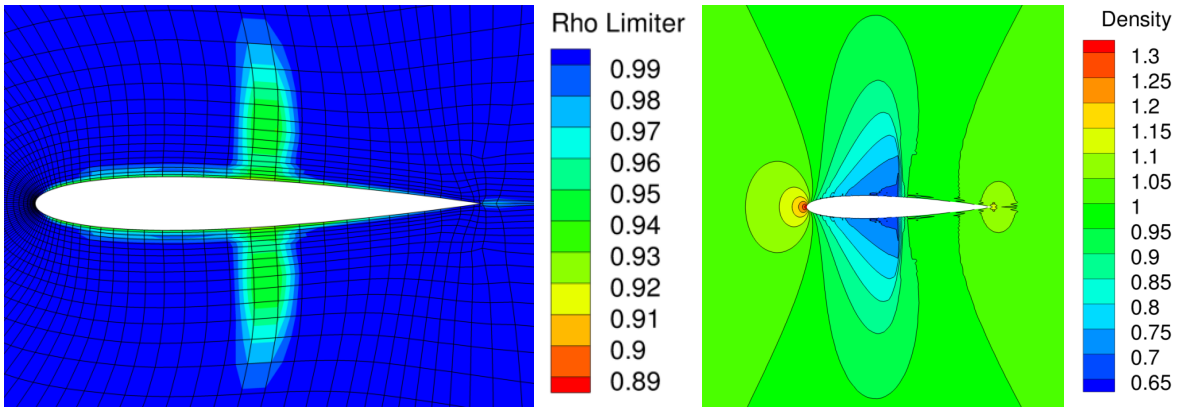

(a) Limited cells for density reconstruction. (b) Density contours.

Figure 4. Results for the SD method NACA 0012 airfoil simulations at $M_\infty = 0.8$ and $\alpha = 0$ deg.

4.2 Supersonic Flow in a Duct

Here the simulation is a uniform supersonic flow encountering a 15 deg. half-angle wedge. This configuration create an oblique shock wave with a 45.34 deg, this shock wave is reflected in the top wall of the duct and then another reflection will happen near the outlet. The freestream Mach number is $M_\infty = 2.0$, the mesh configuration has 96 and 32 cells. The computational mesh is shown in Fig. 5.

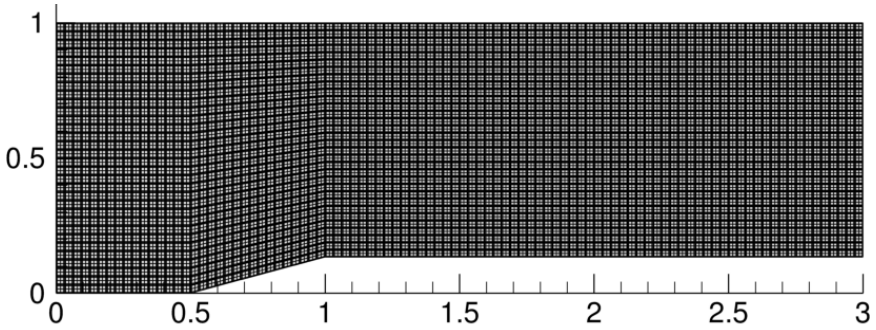

Figure 5. Mesh used for the SD duct simulation for the 3rd-order and 4th-order cases.

The results in this section are for the 3rd-order and 4th-order SD method with the limiting procedure described in the section 3. In the figures 6 - 9, it is shown the density marker and density contours, besides the values for the limiting final parameter of the Eq. 25 is plotted.

The contours of density for the 3-rd SD scheme and for the 4-th SD scheme, are shown, respectively in Fig. 6 and in Fig. 8. The contours are very similar, the value of density is a little higher for the 3-rd scheme, after the shock reflection on the top wall. In both figures the two shock are very well defined, in the 4-th order scheme the contours are more defined in top right corner near the outlet. Also the width of shock seems to be minor for third order.

In the figures 7 and the 9 it is shown the values of the parameter $\tilde{\Phi}_k$ from Eq. 25. This a measure of how much is the cell “limited". By the legend of both figures there is not cells fully limited, i.e., cells with $\tilde{\Phi}_k = 1$. Besides, just a few cells are limited, it seems that a small quantity of cells at the smooth flow are limited, but the solution was not degrade, thus the overall result could be considered a great solution.

For this specific case the limiter has a great overall performance. As mentioned earlier, almost none of cells in the smooth solution are limited. Besides, the function of limiting cells does not present a high value, which could degrade the overall solution considering that the flow in this case are not present a strong shock, i.e., it was expected that the limiter

parameter would not so high.

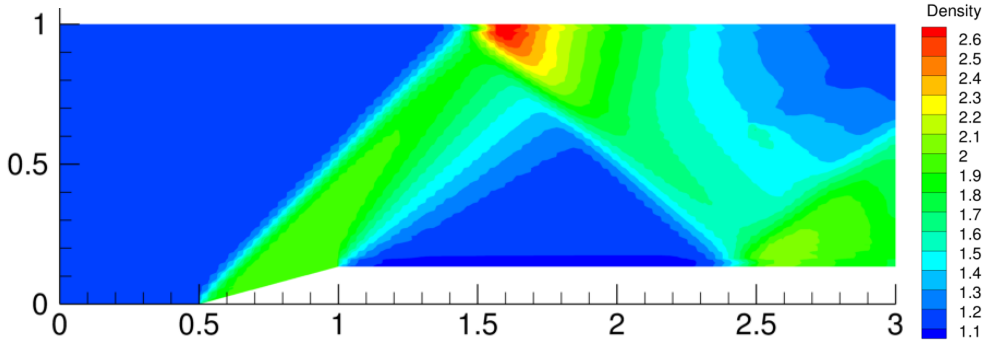

Figure 6. Density contours for a supersonic flow in a duct 3rd-order SD scheme

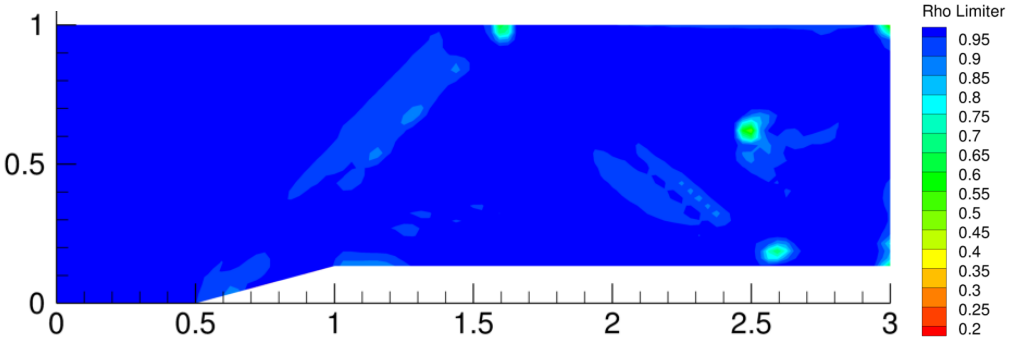

Figure 7. Values for the final limiting parameter 3rd-order SD scheme

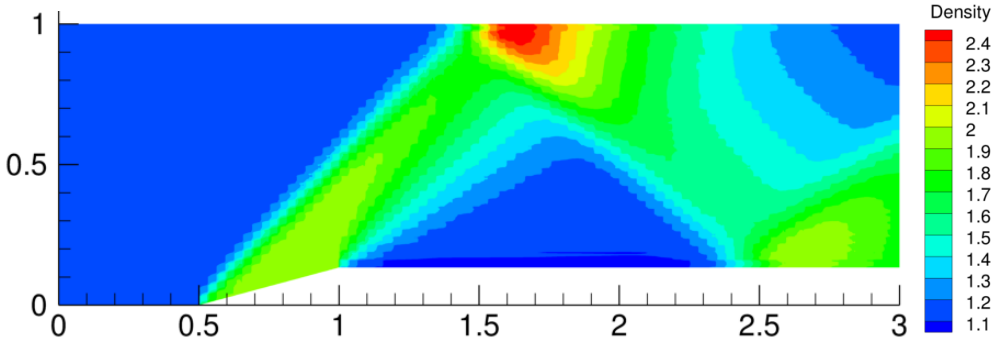

Figure 8. Density contours for a supersonic flow in a duct 4th-order SD scheme

5. CONCLUDING REMARKS

The present work has provided an overview of the current status of the effort undertaken in order to develop a new limiter formulation, adapted for the spectral finite volume method, that would allow the simulation of aerodynamic flows with high-order CFD methods. The present limiter formulation has been obtained by adapting a limiter previously developed for standard finite volume method and for high-order CPR schemes. It is clear that many of the limiting concepts previously developed for low-order schemes do have difficulties when implemented in a high-order method context. The results regarding the hierarchical limiter, see Fig. 3, have demonstrated some of these drawbacks. For further information see the references Moreira *et al.* (2015) and Moreira *et al.* (2016).

The implementation of the new limiter has been performed and verified, still necessary other computational studies to assess the limiter performance for the aerospace-like test cases of interest, such as the convergence rate. But the capability of avoiding limitation of smooth regions of the flow and a comparative with the results with the hierarchical limiter have been here discussed.

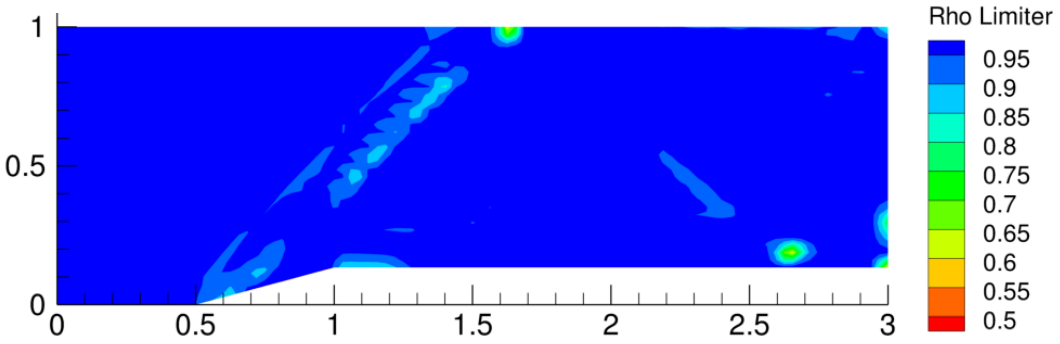

Figure 9. Values for the final limiting parameter 4th-order SD scheme

The results obtained demonstrate that the limiting procedure described here is better than the previous results obtained by other works such as Moreira *et al.* (2015) and Moreira *et al.* (2016). The evolution regarding the new limiter is the limitation of the cells near the extrema, the definition of the shock wave and the non-degradation of the smooth solution. It still necessaries more cases to validate the limiter, but the results here present satisfactory results for some aerospace applications. By now, the major drawback of the proposed limiter is the cells near the wall which are almost fully limited. This feature could indicated that the wall could influences the limiting function, a future work is necessary to determine the reasons of these deficiency.

6. ACKNOWLEDGMENTS

The authors gratefully acknowledge the support for the present research provided by Conselho Nacional de Desenvolvimento Científico e Tecnológico, CNPq, under the Research Grants No. 309985/2013-7, No. 400844/2014-1 and No. 443839/2014-0. The work is also supported by Fundação de Amparo à Pesquisa do Estado de São Paulo, FAPESP, under Research Grant No. 2013/07375-0. The support provided by Fundação Coordenação de Aperfeiçoamento de Pessoal de Nível Superior, CAPES, through graduate scholarships for the first and second authors, is also greatly appreciated.

7. REFERENCES

Breviglieri, C., Azevedo, J.L.F., Basso, E. and Souza, M.A.F., 2010. "Implicit high-order spectral finite volume method for inviscid compressible flows". *AIAA Journal*, Vol. 48, No. 10, pp. 2365–2376.

Li, Y. and Wang, Z.J., 2017. "Recent progresses in developing a convergent and accuracy preserving limiter for the FR/CPR method". In *55th AIAA Aerospace Sciences Meeting and Exhibit*. AIAA Paper No. 2017-0756, Grapevine, TX.

May, G. and Jameson, A., 2006. "A spectral difference method for the Euler and Navier-Stokes equations on unstructured meshes". In AIAA Paper No. 2006-0304*, Proceedings of the 44th AIAA Aerospace Sciences Meeting*. Reno, NV.

Michalak, C. and Ollivier-Gooch, C., 2009. "Accuracy preserving limiter for the high-order accurate solutions of the Euler equations". *Journal of Computational Physics*, Vol. 228, pp. 8693–8711.

Moreira, F.M., Breviglieri, C. and Azevedo, J.L.F., 2015. "High-order compressible flows simulations with the unstructured spectral difference method". In AIAA Paper No. 2015-3195*, Proceedings of the 22nd AIAA Computational Fluid Dynamics Conference*. Dallas, TX.

Moreira, F.M., Jourdan, E., Breviglieri, C., Aguiar, A.R.B. and Azevedo, J.L.F., 2016. "Implicit spectral difference method solutions for compressible flows considering high-order meshes". In AIAA Paper No. 2016-3352*, Proceedings of the 46th AIAA Fluid Dynamics Conference*. Washington, DC.

Persson, P. and Peraire, J., 2006. "Sub-cell shock capturing for discontinuous Galerkin methods". In AIAA Paper No. 2006-0112*, 44th AIAA Aerospace Sciences Meeting and Exhibit*. Reno, NV.

Spitieri, R.J. and Ruuth, S.J., 2003. "A new class of optimal high-order strong-stability-preserving time discretization methods". *SIAM Journal on Numerical Analysis*, Vol. 40, No. 2, pp. 469–491.

Van den Abeele, K., Lacor, C. and Wang, Z.J., 2008. "On the stability and accuracy of the spectral difference method". *Journal of Scientific Computing*, Vol. 37, No. 2, pp. 162–188.

van Leer, B., 1979. "Towards the ultimate conservative difference scheme. V. A second-order sequel to Godunov's method". *Journal of Computational Physics*, Vol. 32, No. 1, pp. 101–136.

Wang, Z.J., Fidkowski, K., Abgrall, R., Bassi, F., Caraeni, D., Cary, A., Deconinck, H., Hartmann, R., Hillewaert, K., Huynh, H.T., Kroll, N., May, G., Persson, P., van Leer, B. and Visbal, M., 2013. "High-order CFD methods: Current status and perspective". *International Journal for Numerical Methods in Fluids*, Vol. 72, No. 8, pp. 811–845.

Wang, Z.J., Liu, Y., May, G. and Jameson, A., 2007. "Spectral difference method for unstructured grids II: Extension to the Euler equations". *Journal of Scientific Computing*, Vol. 32, No. 1, pp. 3938–3956.

Yang, M. and Wang, Z.J., 2009. "A parameter-free generalized moment limiter for high-order methods on unstructured grids". *Advances in Applied Mathematics and Mechanics*, Vol. 1, No. 4, pp. 451–480.

8. RESPONSIBILITY NOTICE

The authors are the only responsible for the printed material included in this paper.